CLIMATOLOGY

Overlooked possibility of a collapsed Atlantic Meridional Overturning Circulation in warming climate

Wei Liu,[1]*† Shang-Ping Xie,[1] Zhengyu Liu,[2] Jiang Zhu[2]

Changes in the Atlantic Meridional Overturning Circulation (AMOC) are moderate in most climate model projections under increasing greenhouse gas forcing. This intermodel consensus may be an artifact of common model biases that favor a stable AMOC. Observationally based freshwater budget analyses suggest that the AMOC is in an unstable regime susceptible for large changes in response to perturbations. By correcting the model biases, we show that the AMOC collapses 300 years after the atmospheric CO_2 concentration is abruptly doubled from the 1990 level. Compared to an uncorrected model, the AMOC collapse brings about large, markedly different climate responses: a prominent cooling over the northern North Atlantic and neighboring areas, sea ice increases over the Greenland-Iceland-Norwegian seas and to the south of Greenland, and a significant southward rain-belt migration over the tropical Atlantic. Our results highlight the need to develop dynamical metrics to constrain models and the importance of reducing model biases in long-term climate projection.

INTRODUCTION

Current climate models suffer from biases (*1*), and therefore, it is critically important to assess the potential impact of the model biases on future climate projections. One vital player for climate change is the Atlantic Meridional Overturning Circulation (AMOC). With a warm, northward near-surface flow and a colder, southward return flow at depth (*2*), the AMOC carries oceanic heat northward and contributes moderate climate to the U.K. and northwest Europe (*3*). There is evidence that the AMOC has slowed down since the early 20th century, although this long-term declining trend of AMOC strength is subject to great uncertainty (*3*). Under future global warming, the AMOC is predicted to further weaken (*1*, *4*–*8*), but the degree of the change is uncertain, ranging from a moderate slowdown (*4*–*7*) to a complete shutdown (*8*). These different AMOC responses essentially depend on the circulation stability (*1*–*3*). Recent studies (*9*–*14*) point to a serious bias in AMOC stability in current climate models. Observational analyses (*9*–*16*) suggest an unstable modern AMOC (with multiple equilibria), meaning that the AMOC may switch between "on" and "off" modes in the future, as it did in the past (*17*–*20*). However, climate models show a common bias toward a stable AMOC (with a single equilibrium) (*21*, *22*). This bias in AMOC stability casts serious doubt on the projection of future AMOC change.

To test the bias impact on future AMOC change, we conduct parallel experiments based on the same climate model but of two versions: the present-day control run (CTL) of the National Center for Atmospheric Research (NCAR) Community Climate System Model version 3 (CCSM3) (*23*, *24*) and a bias adjusted run (ADJ) (*14*) via a surface flux adjustment (see Materials and Methods for details). We further rely on an indicator ΔM^*_{ov} (*25*, *26*) to analyze the stability of the AMOC, which is defined as the difference of the AMOC-induced freshwater transports across the southern (M^*_{ovS}) and northern (M^*_{ovN}) boundaries of the Atlantic (see Materials and Methods for details). Previously, M^*_{ovS} has been used as an AMOC stability indicator (*7*, *10*–*13*, *27*), but it is not an accurate measure of AMOC stability (*26*) because it neglects the freshwater transport between the Atlantic and the Arctic (M^*_{ovN}). For example, Weaver *et al.* (*7*) show that few models in the Coupled Model Intercomparison Project Phase 5 (CMIP5) (*28*) exhibit a rapid collapse of future AMOC, although M^*_{ovS} classifies 40% of them as being in an unstable regime. By contrast, ΔM^*_{ov} accurately denotes the freshwater transport induced by the AMOC and therefore can better represent a basin-wide salt-advection feedback and the AMOC stability (*26*). In particular, a divergence of the AMOC-induced freshwater transport ($\Delta M^*_{ov} < 0$) indicates an unstable AMOC in response to buoyancy perturbation owing to a positive feedback with salinity advection. We suppose that an energetic modern AMOC induces a freshwater divergence. Under global warming conditions, an initial buoyancy perturbation in the North Atlantic weakens the AMOC and hence the associated freshwater divergence. The reduced freshwater divergence may then lead to an accumulation of freshwater in the North Atlantic, further amplifying the initial freshwater perturbation and resulting in a collapse of the AMOC.

RESULTS

Figure 1A shows modern AMOC stability inferred from ΔM^*_{ov} in observations (reanalysis data) (see Materials and Methods for details) and model simulations (table S1). The observations suggest a freshwater divergence induced by a vigorous AMOC ($\Delta M^*_{ov} < 0$) and thus an unstable AMOC, whereas climate models (without flux adjustment, see Materials and Methods for details) simulate a freshwater convergence ($\Delta M^*_{ov} > 0$) and therefore a stable AMOC. This bias in AMOC stability (ΔM^*_{ov}) is mostly caused by a biased M^*_{ovS} because M^*_{ovN} is consistently negative in both observations and models, as associated with a freshwater import from the Arctic (Fig. 1B). At the southern boundary, observations suggest a strong freshwater export owing to a saltier northward flow (Fig. 2B) of surface and thermocline waters (<500 m) than the deep southward flow (Fig. 2B) of the North Atlantic Deep Water (NADW) (1500 to 4000 m), whereas climate models show a freshwater import or a diminished transport primarily due to a fresh bias in salinity above 500 m (Fig. 2A).

The flux adjustment enables a correction of AMOC stability. By eliminating the salinity bias in the upper levels of the South Atlantic (Fig. 2A), the ADJ simulates a strong freshwater export across the southern boundary, an Atlantic freshwater divergence, and therefore an unstable AMOC consistent with observations (Fig. 1, A and B).

[1]Department of Climate, Atmospheric Science and Physical Oceanography, Scripps Institution of Oceanography, University of California, San Diego, La Jolla, CA 92093, USA. [2]Department of Atmospheric and Oceanic Sciences and Center for Climatic Research, University of Wisconsin-Madison, Madison, WI 53705, USA.
*Present address: Department of Geology and Geophysics, Yale University, New Haven, CT 06511, USA.
†Corresponding author. Email: wliu@yale.edu

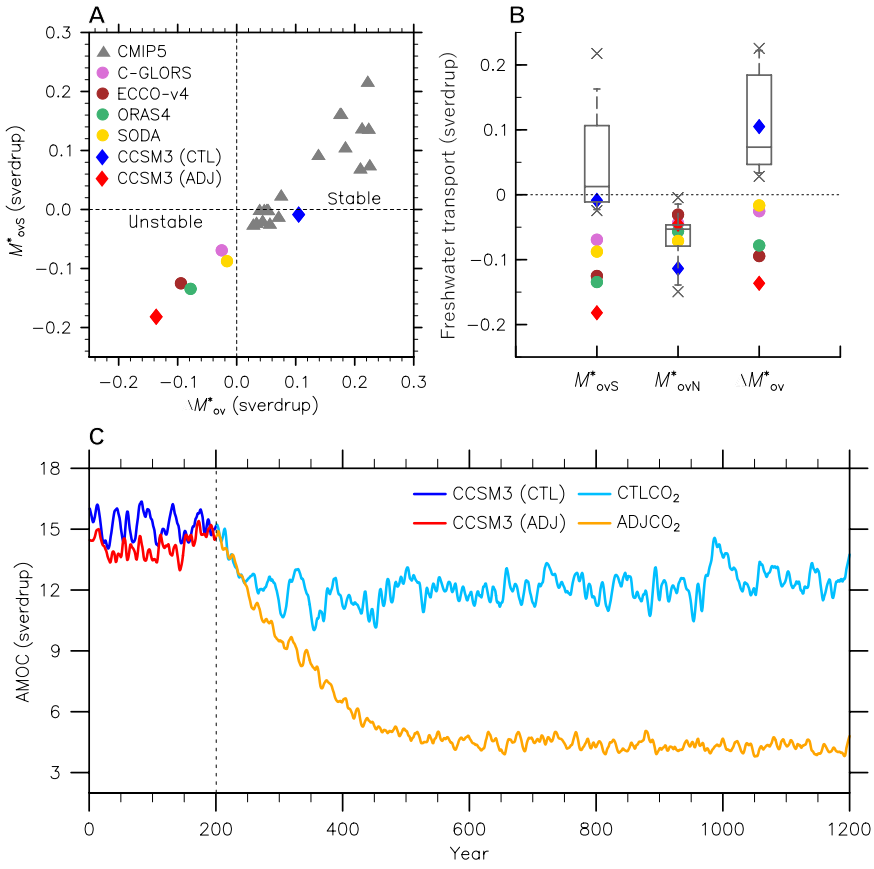

Fig. 1. AMOC stability in modern climate and AMOC response under global warming. (**A**) AMOC stability diagram where M^*_{ovS} and M^*_{ov} are the AMOC stability indicators defined in Materials and Methods. The indicator values in modern climate are shown in solid circles for reanalysis data [Centro Euro-Mediterraneo sui Cambiamenti Climatici Global Ocean Physical Reanalysis System (C-GLORS; pink), Estimating the Circulation and Climate of the Ocean version 4 (ECCO-v4; brown), Ocean Reanalysis System 4 (ORAS4; green), and Simple Ocean Data Assimilation (SODA; yellow)], in gray triangles for the CMIP5 model simulations, and in blue and red diamonds for the CCSM3 CTL and ADJ runs. A positive or negative ΔM^*_{ov} indicates that the AMOC resides in a stable or unstable regime. (**B**) M^*_{ovS}, ΔM^*_{ovN}, and ΔM^*_{ov} from reanalysis data, the CCSM3 CTL and ADJ runs with the same marker and color scheme as in (A), and the CMIP5 climate models in the form of the box-and-whisker plot. (**C**) Evolution of AMOC strength in the CTL (blue), $CTLCO_2$ (light blue), ADJ (red), and $ADJCO_2$ (orange), where the AMOC strength is defined as the maximum in the stream function below 500 m in the North Atlantic. A locally weighted scatterplot smoothing of 10-year intervals is applied to annual mean AMOC strength to remove interannual variability.

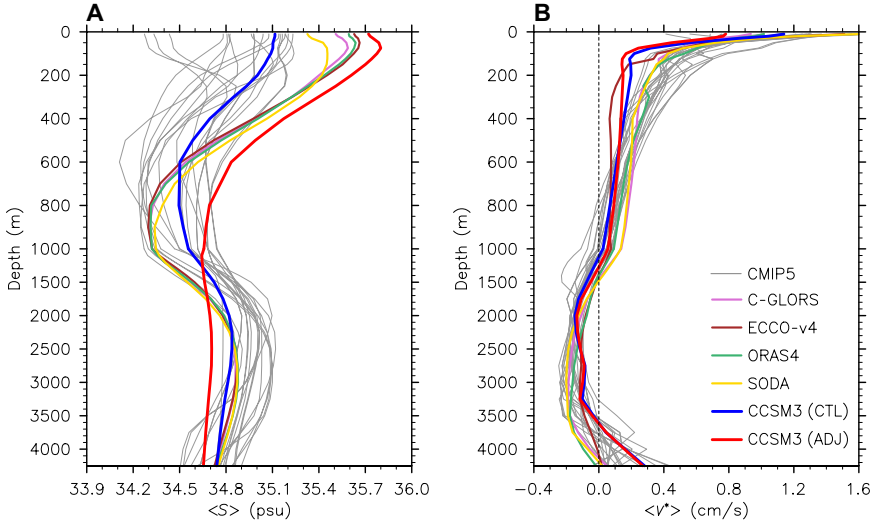

Fig. 2. Salinity and velocity profiles. Zonal mean (**A**) salinity and (**B**) baroclinic meridional velocity at the southern boundary (~34°S) of the Atlantic as a function of depth. psu, practical salinity units. Annual mean results are calculated from reanalysis data [C-GLORS (pink), ECCO-v4 (brown), ORAS4 (green), and SODA (yellow)], the CMIP5 model simulations (gray), and the CCSM3 CTL (blue) and ADJ (red) runs.

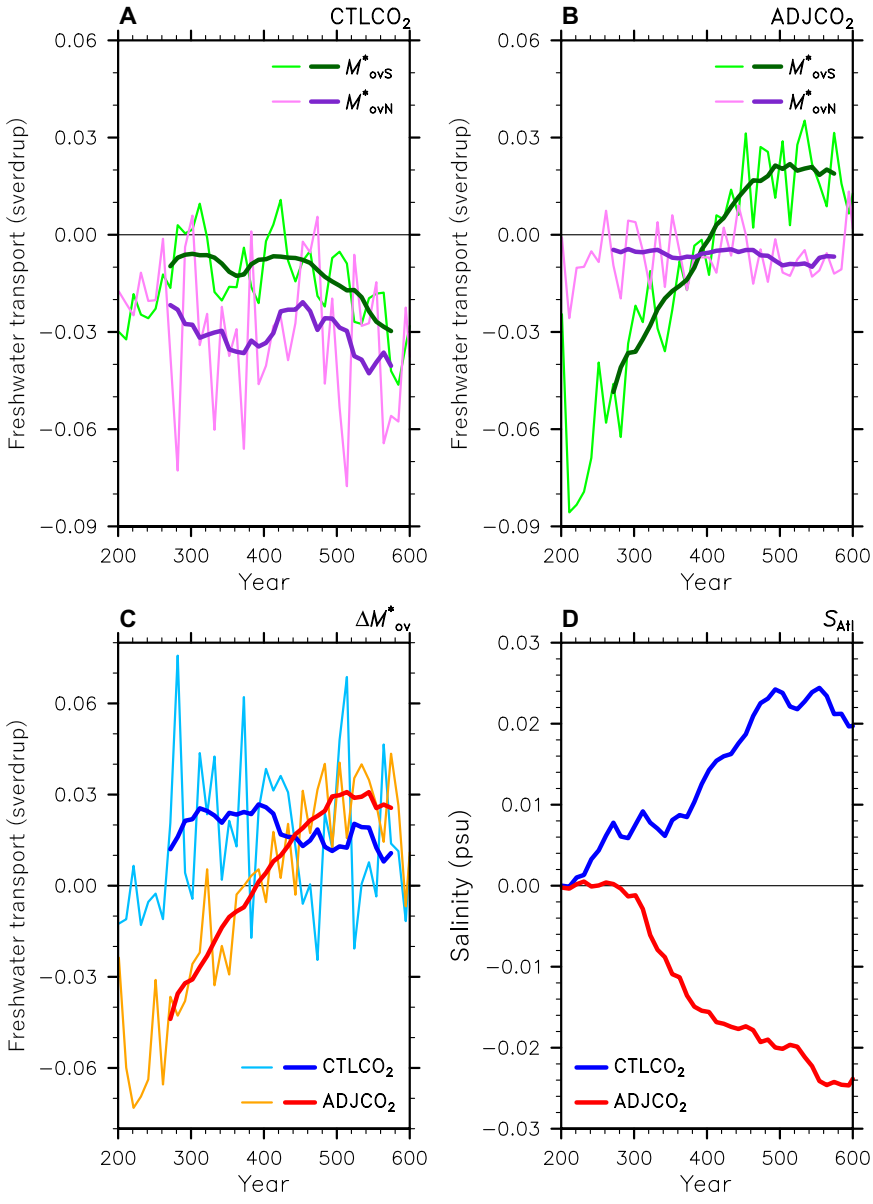

Fig. 3. Evolutions of freshwater transport and salinity. Decadal mean anomalies in double CO_2 simulations (relative to the climatology in the CTL and ADJ) for freshwater transports M^*_{ovS} (light green) and M^*_{ovN} (pink) in (**A**) the $CTLCO_2$ and (**B**) $ADJCO_2$, for (**C**) ΔM^*_{ov} in the $CTLCO_2$ (light blue) and $ADJCO_2$ (orange), and for (**D**) the Atlantic basin mean salinity ΔS_{Atl} in the $CTLCO_2$ (blue) and $ADJCO_2$ (red). A 90-year running mean is applied to M^*_{ovS}, M^*_{ovN}, and ΔM^*_{ov} during years 251 to 600, with results shown in thick lines. Smoothed M^*_{ovS} (dark green) and M^*_{ovN} (purple) are shown in (A) and (B), whereas smoothed ΔM^*_{ov} is shown in (C), in blue for the $CTLCO_2$ and in red for the $ADJCO_2$.

Meanwhile, the flux adjustment only slightly modulates the magnitude of the AMOC. The AMOC volume transport remains similar in both CTL and ADJ (fig. S1, A and C) and close to observations (*29*).

We conduct two parallel doubling CO_2 experiments (the $CTLCO_2$ and $ADJCO_2$) based on two versions of the CCSM3 (see Materials and Methods for details). The atmospheric CO_2 concentration is instantaneously doubled (at year 201) from the present-day level and then remains constant thereafter. This warming scenario is between the Representative Concentration Pathways (RCP) 4.5 and RCP6.0 scenarios from the Intergovernmental Panel on Climate Change Fifth Assessment Report (*1*). The two models show similar climate responses during the first three decades. The AMOC strength reduces (Fig. 1C), and the Arctic sea ice shrinks (fig. S2B). The surface warming pattern is consistent with observations, which is characterized as a warming minimum (or slight cooling) to the south of Greenland, intensified warming over Eurasia and North America, and enhanced warming in the tropical Pacific, with a warming minimum in the southeastern Pacific (fig. S3). Nevertheless, predictions by the two models diverge markedly after the first 50 years. In the $CTLCO_2$, the AMOC slightly and slowly recovers (Fig. 1C), which is consistent with projections by most CMIP5 models (*6*, *7*). In the $ADJCO_2$, by contrast, the AMOC continues to decelerate and eventually collapses at year 500 (Fig. 1C). These distinct AMOC behaviors between models originate from the AMOC stability. During years 251 to 500, the initial weakening of the AMOC in the $ADJCO_2$ ($CTLCO_2$) causes an anomalous freshwater divergence (convergence) in the Atlantic (Fig. 3C), primarily through the transport change across the southern boundary (Fig. 3, A and B). This

freshens (salinifies) the Atlantic (Fig. 3D), inhibits (promotes) the deep convection and NADW formation, and finally leads to a collapse (partial recovery) of the AMOC. It is worth mentioning that ΔM^*_{ov} in the $ADJCO_2$ eventually switches from negative to positive, implying that the evolving AMOC acts to accumulate freshwater in the Atlantic and, thus, the final collapsed state is steady.

The distinct AMOC changes between the $ADJCO_2$ and $CTLCO_2$ cause distinct long-term climate responses. For example, during years 251 to 500, in the $ADJCO_2$ ($CTLCO_2$), sea ice area increases (decreases) in the Northern Hemisphere (fig. S2B). We further examine the centurial mean difference between the $ADJCO_2$ ($CTLCO_2$; years 501 to 600) and the ADJ (CTL; years 101 to 200). The $ADJCO_2$ predicts a large cooling over the northern North Atlantic and neighboring areas (Fig. 4C). Surface air temperatures over the U.K., Iceland, and northwest Europe can drop to greater than 7°C during boreal winter. Associated with this cooling, sea ice expands over the Greenland-Iceland-Norwegian (GIN) seas and to the south of Greenland (fig. S4C). Compared with the $CTLCO_2$, the $ADJCO_2$ predicts a general cooling in the Northern Hemisphere polar region to 45°N (Fig. 4E), and sea ice retreat (fig. S4D) around Antarctica. The global mean surface air temperature in the $ADJCO_2$ is ~0.4°C less than that in the $CTLCO_2$ (fig. S2A).

The effect of flux adjustment on climate change extends into the tropics. Unlike the $CTLCO_2$, the $ADJCO_2$ simulates a stronger (weaker) surface warming south (north) of the equator in the Atlantic (Fig. 4C),

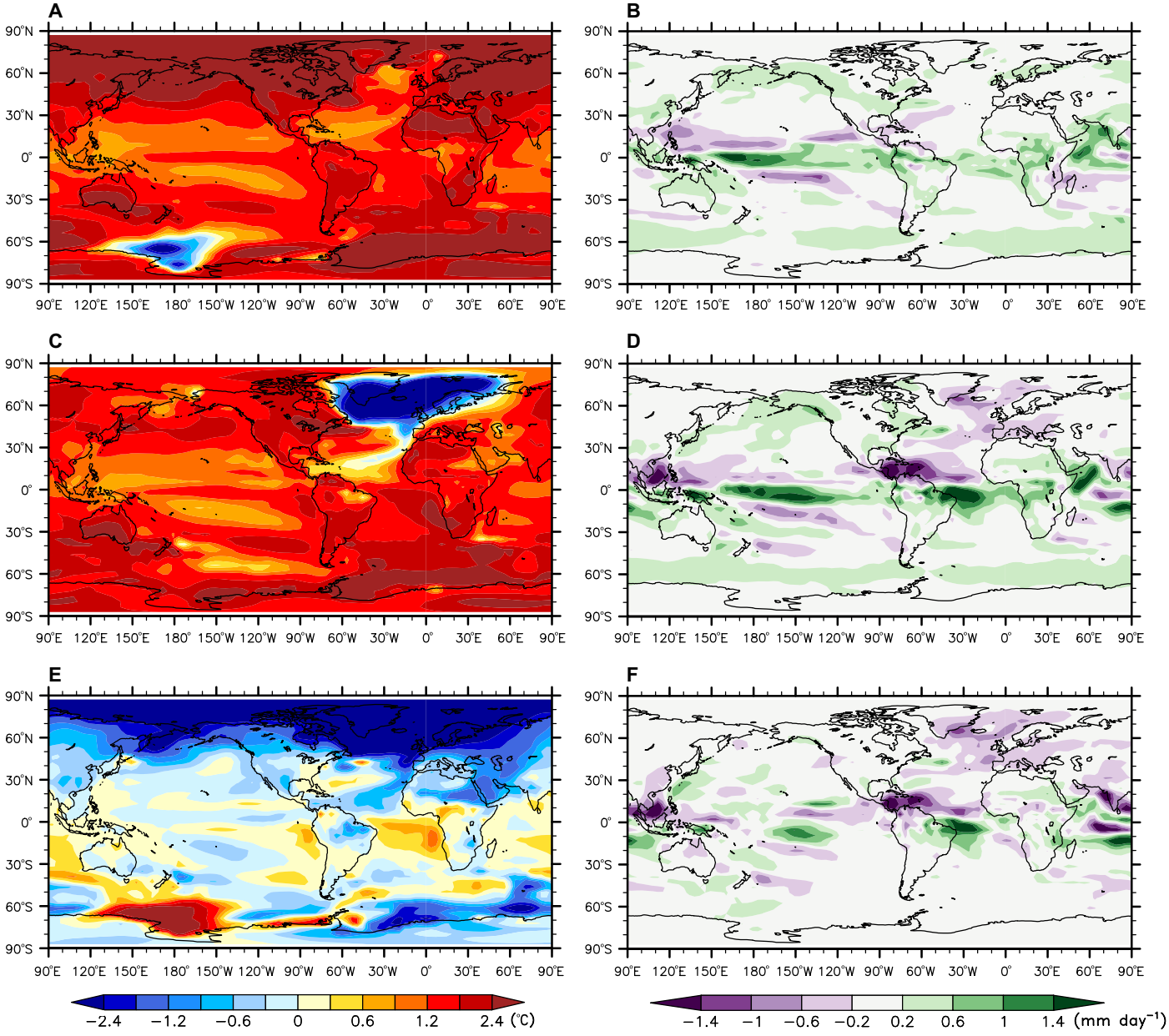

Fig. 4. Long-term (after 300 years) responses of surface temperature and precipitation to CO_2 increase. (**A**, **C**, and **E**) Results of annual mean temperature (shading in °C): (A) the $CTLCO_2$ minus the CTL (C) the $ADJCO_2$ minus the ADJ, and (E) the difference between (C) and (A). (**B**, **D**, and **F**) Similar to (A), (C), and (E) but for the results of annual mean precipitation (shading in mm day^{-1}).

as caused by a severe decline in the AMOC and associated heat transport. The warming pattern effectively displaces the Altantic Inter-tropical Convergence Zone (ITCZ) southward and generates a rainfall dipole astride the equator: enhanced precipitation over the tropical South Atlantic and northeastern Brazil and reduced precipitation over the tropical North Atlantic and Central America (Fig. 4D). This ITCZ shift corresponds to a robust southward migration of the Hadley cell (fig. S5). Overall in the tropics, the difference in rainfall change between the $ADJCO_2$ and $CTLCO_2$ runs closely follows the patterns of SST difference (Fig. 4, E and F) (*30*).

DISCUSSION

We have used a bias correction approach to illustrate the impact of the AMOC stability bias on future climate projections. The corrections put the AMOC in an unstable regime and lead to an AMOC collapse 300 years after a CO_2 doubling. With the AMOC shutdown, the bias-adjusted model predicts a distinct climate change from most CMIP5 models: a prominent cooling over the northern North Atlantic and neighboring areas, a remarkable sea ice expansion over the GIN seas and to the south of Greenland, and a significant southward rain-belt migration over the tropical Atlantic. Our results suggest that prevailing predictions by the CMIP5 models underestimate the model uncertainty in AMOC response and regional climate change around the North Atlantic.

The same model simulates an AMOC collapse with a large 1-sverdrup (1 sverdrup = 10^6 m^3/s) freshwater pulse (*14*) that mimics major ice-sheet discharges into the North Atlantic in paleoclimate observations. The AMOC collapse is primarily caused by a halinely induced reduction of surface buoyancy (see fig. S6F and Materials and Methods for details) associated with an extreme freshening in the northern North Atlantic and GIN seas (fig. S6L). On the other hand, the current study uses a more realistic setting, that is, the CO_2 increase for future global warming. The AMOC shutdown under global warming is primarily caused by a thermally induced buoyancy reduction (fig. S6B). The resultant buoyancy change (fig. S6A) is about one order of magnitude smaller (~0.1 sverdrup) than that in the hosing experiment (fig. S6D). Another important difference between the global warming and hosing scenarios is the response of atmospheric moisture transport from the Atlantic to the Pacific across Central America. Under global warming, the moisture transport intensifies because of atmospheric moisture increase, a negative feedback that increases Atlantic salinity (*31*) and stabilizes the AMOC (*32*–*34*). However, this mechanism is generally absent in the hosing experiments (*34*).

MATERIALS AND METHODS

The NCAR CCSM3 simulations

We used the NCAR CCSM3 (*23*) with the T31_gx3v5 resolution (nominally 3°, with significantly finer resolution toward Greenland) (*24*), a climate model without flux adjustment. The CTL was adopted from a 200-year simulation (years 1001 to 1200) in the CCSM3 control run in the perpetual 1990 scenario and redenoted as years 1 to 200. Corresponding to the CTL, the ADJ was built via a classical flux adjustment approach (*35*) in which the model surface temperature and salinity climatologies were adjusted toward observations using a seasonal cycle of anomalous heat and freshwater fluxes (*14*). The artificially added heat and freshwater fluxes eliminated most temperature and salinity biases at the ocean surface (fig. S7), potentially improving the formation area of NADW (fig. S8, A to C) and the simulation of Atlantic multidecadal oscillation, which was associated with AMOC variability (fig. S8, D to G). Model years in the ADJ were redenoted from 1 to 200. Herein, we would like to clarify that the reason for introducing flux adjustments was the substantial AMOC stability bias in climate models. The flux adjustments were meant to explore the possible range of AMOC response as a function of AMOC stability, but they were by no means the solution to a realistic solution for the AMOC. The results need to be tested with physically improved models.

From year 201, two parallel double CO_2 experiments (the $CTLCO_2$ and $ADJCO_2$) were conducted, in which atmospheric CO_2 concentration was instantaneously doubled from the 1990 level and then fixed. It merits attention that the meltwater discharge from the Greenland ice sheet is not included in the double CO_2 experiments; thus, the behavior of the AMOC is entirely under radiative forcing due to increasing CO_2. Our results suggest a possibility of future AMOC collapse without ablation of the Greenland ice sheet. Also, a strong regional cooling was found in the $ADJCO_2$ over the northern North Atlantic 300 years after CO_2 doubling. This is because an extreme AMOC weakening causes a striking local cooling that overcomes the global warming induced by CO_2 increase. Here, the CO_2 doubling is a modest warming scenario between the RCP4.5 and RCP6.0 scenarios. Our results may alter if an extreme warming scenario, for example, the RCP8.5 scenario, is adopted.

In addition, a hosing experiment from a previous study (*14*) was used for comparisons with $ADJCO_2$. The hosing experiment (ADJHOS) was based on the ADJ, with a strong freshwater perturbation of 1 sverdrup imposed over the high-latitude North Atlantic (50°N to 70°N) from year 201. The freshwater perturbation was terminated after 100 years.

The AMOC stability indicator

A dynamical metric named ΔM^*_{ov} was adopted in the study, which is related to the freshwater transport induced by the AMOC. In particular, the equivalent freshwater transport associated with the AMOC along a zonal section at latitude (ϕ) is calculated approximately as

$$M^*_{ov}(\phi) = -\frac{1}{S_0}\int_{-D}^{0} \overline{v^*}\,(\phi, z)\langle S(\phi, z)\rangle dz \qquad (1)$$

where S_0 = 34.8 psu is a reference salinity, z represents depth, $-D$ is the depth of the ocean bottom, $v^*(\phi, z)$ is the meridional baroclinic ocean velocity, overbar denotes zonal integral, and $\langle S(\phi, z)\rangle$ denotes the zonal mean salinity. The AMOC stability indicator ΔM^*_{ov} is defined as the difference of the AMOC freshwater transports across the southern and northern boundaries of the Atlantic (*25*, *26*), which can be expressed as

$$\Delta M^*_{ov} = M^*_{ovS} - M^*_{ovN} \qquad (2)$$

where M^*_{ovS} denotes the transport at the southern boundary of the Atlantic (~34°S), which served as a candidate of the AMOC stability indicator in early studies (*7*, *10*–*13*, *27*). M^*_{ovN} denotes the transport at the northern boundary of the Atlantic (~80°N), which is equal to the sum of overturning components of liquid freshwater import from the Arctic ocean via three sections: the Canadian Arctic Archipelago (M^*_{ovCAA}), the Fram Strait (M^*_{ovFRA}), and the western shelf of the Barents Sea (M^*_{ovBAR}). Calculation of M^*_{ovCAA}, M^*_{ovFRA}, and M^*_{ovBAR} follows the formulation of M^*_{ov} but with v^* normal to section, integration, and averaging carried along the direction of each section. Here, climatologically annual mean values of ΔM^*_{ov}, M^*_{ovS}, and M^*_{ovN} are calculated from

monthly outputs of reanalysis data sets, the CMIP5 model simulations, and the CCSM3 CTL and ADJ runs.

Observational data

We used the National Oceanic and Atmospheric Administration Extended Reconstructed Sea Surface Temperature (SST) version 4 (ERSST.v4) (*36*, *37*) during 1854 to 2014, Monthly Isopycnal/Mixed-layer Ocean Climatology (MIMOC) (*38*), NASA Goddard Institute for Space Studies Surface Temperature Analysis (GISTEMP) (*39*) during 1880 to 2014, and reanalysis data during the span of 1970 to 2014: the C-GLORS (*40*) during 1982 to 2013, ECCO-v4 release 2 (*41*) during 1992 to 2011, the European Centre for Medium-Range Weather Forecasts ORAS4 (*42*) during 1970 to 2014, and SODA version 2.2.4 (*43*) during 1970 to 2008.

The CMIP5 simulations

We used monthly outputs during 1970 to 2005 from the historical runs (*28*) of 20 CMIP5 climate models (table S1). The simulations were driven by historical changes in well-mixed greenhouse gases, aerosols, and stratospheric ozone depletion. No flux adjustment was adopted in these models.

The surface density flux

The surface density flux, a measure of the loss/gain of water mass of the ocean surface layer due to the heat and freshwater exchanges (*44*), was examined in the ADJ, ADJCO$_2$, and ADJHOS. The density flux (DF) is calculated as

$$\mathrm{DF} = -\alpha\frac{Q}{C_p} + \rho(0,\mathrm{SST})\beta\frac{(E-P-R-I)\mathrm{SSS}}{1-\mathrm{SSS}} \qquad (3)$$

where the first term $-\alpha\frac{Q}{C_p}$ represents the thermal contribution (denoted as TF), and the second term $\rho(0,\mathrm{SST})\beta\frac{(E-P-R-I)\mathrm{SSS}}{1-\mathrm{SSS}}$ represents the haline contribution (denoted as SF). C_p, SST, and SSS are the specific heat capacity, sea surface temperature, and sea surface salinity, respectively. α and β are the thermal expansion and haline contraction coefficients. $\rho(0, \mathrm{SST})$ is the density of freshwater with salinity of 0 and temperature of SST. Q represents the net surface heat flux, and E, P, R, and I denote the freshwater fluxes due to evaporation, precipitation, river runoff, and sea ice melting and brine rejection, respectively.

SUPPLEMENTARY MATERIALS

Supplementary material for this article is available at http://advances.sciencemag.org/cgi/content/full/3/1/e1601666/DC1

fig. S1. The depth and latitude diagram of annual mean AMOC stream function.
fig. S2. Annual mean anomalies in double CO$_2$ simulations.
fig. S3. Short-term (0 to 30 years) surface temperature response to CO$_2$ increase.
fig. S4. Long-term (after 300 years) response of sea ice coverage to CO$_2$ increase.
fig. S5. Response of the Hadley cell 300 years after CO$_2$ increase.
fig. S6. Changes in the surface fluxes and variables over the North Atlantic in the first 30 years after CO$_2$ increase.
fig. S7. Annual mean SST and SSS biases.
fig. S8. Observed and simulated formation areas of NADW and Atlantic multidecadal oscillation.
table S1. The CMIP5 models used in this study and their sponsors, countries, and names.

REFERENCES AND NOTES

1. IPCC, *Climate Change 2013: The Physical Science Basis, Contribution of Working Group I to the Fifth Assessment Report of the Intergovernmental Panel on Climate Change* (Cambridge Univ. Press, Cambridge, 2013).
2. M. A. Srokosz, H. L. Bryden, Observing the Atlantic Meridional Overturning Circulation yields a decade of inevitable surprises. *Science* **348**, 1255575 (2015).
3. M. W. Buckley, J. Marshall, Observations, inferences, and mechanisms of the Atlantic Meridional Overturning Circulation: A review. *Rev. Geophys.* **54**, 5–63 (2016).
4. J. M. Gregory, K. W. Dixon, R. J. Stouffer, A. J. Weaver, E. Driesschaert, M. Eby, T. Fichefet, H. Hasumi, A. Hu, J. H. Jungclaus, I. V. Kamenkovich, A. Levermann, M. Montoya, S. Murakami, S. Nawrath, A. Oka, A. P. Sokolov, R. B. Thorpe, A model intercomparison of changes in the Atlantic thermohaline circulation in response to increasing atmospheric CO$_2$ concentration. *Geophys. Res. Lett.* **32**, L12703 (2005).
5. M. A. Rugenstein, M. Winton, R. J. Stouffer, S. M. Griffies, R. Hallberg, Northern high-latitude heat budget decomposition and transient warming. *J. Clim.* **26**, 609–621 (2013).
6. W. Cheng, J. C. H. Chiang, D. Zhang, Atlantic Meridional Overturning Circulation (AMOC) in CMIP5 models: RCP and historical simulations. *J. Clim.* **26**, 7187–7197 (2013).
7. A. J. Weaver, J. Sedláček, M. Eby, K. Alexander, E. Crespin, T. Fichefet, G. Philippon-Berthier, F. Joos, M. Kawamiya, K. Matsumoto, M. Steinacher, K. Tachiiri, K. Tokos, M. Yoshimori, K. Zickfeld, Stability of the Atlantic meridional overturning circulation: A model intercomparison. *Geophys. Res. Lett.* **39**, L20709 (2012).
8. A. Schmittner, M. Latif, B. Schneider, Model projections of the North Atlantic thermohaline circulation for the 21st century assessed by observations. *Geophys. Res. Lett.* **32**, L23710 (2005).
9. S. E. Huisman, M. den Toom, H. A. Dijkstra, S. Drijfhout, An indicator of the multiple equilibria regime of the Atlantic Meridional Overturning Circulation. *J. Phys. Oceanogr.* **40**, 551–567 (2010).
10. S. L. Weber, S. S. Drijfhout, A. Abe-Ouchi, M. Crucifix, M. Eby, A. Ganopolski, S. Murakami, B. Otto-Bliesner, W. R. Peltier, The modern and glacial overturning circulation in the Atlantic Ocean in PMIP coupled model simulations. *Clim. Past* **3**, 51–64 (2007).
11. M. Hofmann, S. Rahmstorf, On the stability of the Atlantic meridional overturning circulation. *Proc. Natl. Acad. Sci. U.S.A.* **106**, 20584–20589 (2009).
12. S. S. Drijfhout, S. L. Weber, E. van der Swaluw, The stability of the MOC as diagnosed from model projections from pre-industrial, present and future climates. *Clim. Dyn.* **37**, 1575–1586 (2011).
13. E. Hawkins, R. S. Smith, L. C. Allison, J. M. Gregory, T. J. Woollings, H. Pohlmann, B. de Cuevas, Bistability of the Atlantic overturning circulation in a global climate model and links to ocean freshwater transport. *Geophys. Res. Lett.* **38**, L10605 (2011).
14. W. Liu, Z. Liu, E. C. Brady, Why is the AMOC monostable in coupled general circulation models? *J. Clim.* **27**, 2427–2443 (2014).
15. W. Weijer, W. P. M. de Ruijter, H. A. Dijkstra, P. J. van Leeuwen, Impact of interbasin exchange on the Atlantic overturning circulation. *J. Phys. Oceanogr.* **29**, 2266–2284 (1999).
16. H. L. Bryden, B. A. King, G. D. McCarthy, South Atlantic overturning circulation at 24°S. *J. Mar. Res.* **69**, 38–56 (2011).
17. W. S. Broecker, D. M. Peteet, D. Rind, Does the ocean–atmosphere system have more than one stable mode of operation? *Nature* **315**, 21–26 (1985).
18. S. Rahmstorf, Ocean circulation and climate during the past 120,000 years. *Nature* **419**, 207–214 (2002).
19. P. U. Clark, N. G. Pisias, T. F. Stocker, A. J. Weaver, The role of the thermohaline circulation in abrupt climate change. *Nature* **415**, 863–869 (2002).
20. J. McManus, R. Francois, J.-M. Gherardi, L. D. Keigwin, S. Brown-Leger, Collapse and rapid resumption of Atlantic meridional circulation linked to deglacial climate changes. *Nature* **428**, 834–837 (2004).
21. R. J. Stouffer, J. Yin, J. M. Gregory, K. W. Dixon, M. J. Spelman, W. Hurlin, A. J. Weaver, M. Eby, G. M. Flato, H. Hasumi, A. Hu, J. H. Jungclaus, I. V. Kamenkovich, A. Levermann, M. Montoya, S. Murakami, S. Nawrath, A. Oka, W. R. Peltier, D. Y. Robitaille, A. Sokolov, G. Vettoretti, S. L. Weber, Investigating the causes of the response of the thermohaline circulation to past and future climate changes. *J. Clim.* **19**, 1365–1387 (2006).
22. A. Hu, B. L. Otto-Bliesner, G. A. Meehl, W. Han, C. Morrill, E. C. Brady, B. Briegleb, Response of thermohaline circulation to freshwater forcing under present day and LGM conditions. *J. Clim.* **21**, 2239–2258 (2008).
23. W. D. Collins, C. M. Bitz, M. L. Blackmon, G. B. Bonan, C. S. Bretherton, J. A. Carton, P. Chang, S. C. Doney, J. J. Hack, T. B. Henderson, J. T. Kiehl, W. G. Large, D. S. McKenna, B. D. Santer, R. D. Smith, The Community Climate System Model version 3 (CCSM3). *J. Clim.* **19**, 2122–2143 (2006).
24. S. G. Yeager, C. A. Shields, W. G. Large, J. J. Hack, The low-resolution CCSM3. *J. Clim.* **19**, 2545–2566 (2006).
25. H. A. Dijkstra, Characterization of the multiple equilibria regime in a global ocean model. *Tellus* **59**, 695–705 (2007).
26. W. Liu, Z. Liu, A diagnostic indicator of the stability of the Atlantic Meridional Overturning Circulation in CCSM3. *J. Clim.* **26**, 1926–1938 (2013).
27. S. Rahmstorf, On the freshwater forcing and transport of the Atlantic thermohaline circulation. *Clim. Dyn.* **12**, 799–811 (1996).
28. K. E. Taylor, R. J. Stouffer, G. A. Meehl, An overview of CMIP5 and the experiment design. *Bull. Am. Meteorol. Soc.* **93**, 485–498 (2012).
29. D. A. Smeed, G. D. McCarthy, S. A. Cunningham, E. Frajka-Williams, D. Rayner, W. E. Johns, C. S. Meinen, M. O. Baringer, B. I. Moat, A. Duchez, H. L. Bryden, Observed

decline of the Atlantic meridional overturning circulation 2004–2012. *Ocean Sci.* **10**, 29–38 (2014).
30. S. P. Xie, C. Deser, G. A. Vecchi, J. Ma, H. Teng, A. T. Wittenberg, Global warming pattern formation: Sea surface temperature and rainfall. *J. Clim.* **23**, 966–986 (2010).
31. P. J. Durack, S. E. Wijffels, R. J. Matear, Ocean salinities reveal strong global water cycle intensification during 1950 to 2000. *Science* **336**, 455–458 (2012).
32. M. Latif, E. Roeckner, U. Mikolajewicz, R. Voss, Tropical stabilization of the thermohaline circulation in a greenhouse warming simulation. *J. Clim.* **13**, 1809–1813 (2000).
33. D. Swingedouw, P. Braconnot, P. Delecluse, E. Guilyardi, O. Marti, Quantifying the AMOC feedbacks during a 2×CO_2 stabilization experiment with land-ice melting. *Clim. Dyn.* **29**, 521–534 (2007).
34. I. Richter, S.-P. Xie, Moisture transport from the Atlantic to the Pacific basin and its response to North Atlantic cooling and global warming. *Clim. Dyn.* **35**, 551–566 (2010).
35. S. Manabe, R. J. Stouffer, Two stable equilibria of a coupled ocean-atmosphere model. *J. Clim.* **1**, 841–866 (1988).
36. B. Huang, V. F. Banzon, E. Freeman, J. Lawrimore, W. Liu, T. C. Peterson, T. M. Smith, P. W. Thorne, S. D. Woodruff, H.-M. Zhang, Extended Reconstructed Sea Surface Temperature version 4 (ERSST.v4). Part I: Upgrades and intercomparisons. *J. Clim.* **28**, 911–930 (2015).
37. W. Liu, B. Huang, P. W. Thorne, V. F. Banzon, H.-M. Zhang, E. Freeman, J. Lawrimore, T. C. Peterson, T. M. Smith, S. D. Woodruff, Extended Reconstructed Sea Surface Temperature version 4 (ERSST.v4): Part II. Parametric and structural uncertainty estimations. *J. Clim.* **28**, 931–951 (2015).
38. G. C. Johnson, S. Schmidtko, J. M. Lyman, Relative contributions of temperature and salinity to seasonal mixed layer density changes and late-winter horizontal density gradients. *J. Geophys. Res.* **117**, C04015 (2012).
39. J. Hansen, R. Ruedy, M. Sato, K. Lo, Global surface temperature change. *Rev. Geophys.* **48**, RG4004 (2010).
40. A. Storto, S. Masina, A. Navarra, Evaluation of the CMCC eddy-permitting global ocean physical reanalysis system (C-GLORS, 1982–2012) and its assimilation components. *Q. J. R. Meteorol. Soc.* **142**, 738–758 (2016).
41. G. Forget, J.-M. Campin, P. Heimbach, C. N. Hill, R. M. Ponte, C. Wunsch, ECCO version 4: An integrated framework for non-linear inverse modeling and global ocean state estimation. *Geosci. Model Dev.* **8**, 3071–3104 (2015).
42. M. A. Balmaseda, K. Mogensen, A. T. Weaver, Evaluation of the ECMWF ocean reanalysis system ORAS4. *Q. J. R. Meteorol. Soc.* **139**, 1132–1161 (2013).
43. J. A. Carton, B. A. Giese, Reanalysis of ocean climate using simple ocean data assimilation (SODA). *Mon. Weather Rev.* **136**, 2999–3017 (2008).
44. K. Speer, E. Tziperman, Rates of water mass formation in the North Atlantic Ocean. *J. Phys. Oceanogr.* **22**, 93–104 (1992).

Acknowledgments: We thank T. Delworth for helpful discussions. We thank two anonymous reviewers for their valuable comments that helped improve the manuscript. **Funding:** This work was supported by the NSF, NSFC(41130105), the U.S. Department of Energy, and the Ministry of Science and Technology of the People's Republic of China (2012CB955201). **Author contributions:** W.L. and Z.L. conceived and designed the experiments. W.L. and J.Z. performed the experiments. W.L. and S.-P.X. analyzed the data. W.L., S.-P.X., and Z.L. wrote the manuscript. **Competing interests:** The authors declare that they have no competing interests. **Data and materials availability:** The ERSST.v4 data are publicly available at https://www.ncdc.noaa.gov/data-access/marineocean-data/extended-reconstructed-sea-surface-temperature-ersst-v4. The MIMOC data are publicly available at www.pmel.noaa.gov/mimoc/. The GISTEMP data are publicly available at http://data.giss.nasa.gov/gistemp/. The C-GLORS data are publicly available at www.cmcc.it/c-glors/. The ECCO-v4 data are publicly available at http://www.ecco-group.org. The ORAS4 data are publicly available at https://climatedataguide.ucar.edu/climate-data/oras4-ecmwf-oceanreanalysis-and-derived-ocean-heat-content%20and%20Integrated%20Climate%20Data%20Center%E2%80%93ICDC. The SODA 2.2.4 data are publicly available at https://iridl.ldeo.columbia.edu/SOURCES/.CARTON-GIESE/.SODA/.v2p2p4/index.html?Set-Language=en. The CMIP5 data are publicly available through the portal of the U.S. Earth System Grid Center for Enabling Technologies on the page http://pcmdi9.llnl.gov/. All data needed to evaluate the conclusions in the paper are present in the paper and/or the Supplementary Materials. Additional data related to this paper may be requested from the authors.

Submitted 19 July 2016
Accepted 22 November 2016
Published 4 January 2017
10.1126/sciadv.1601666

Citation: W. Liu, S.-P. Xie, Z. Liu, J. Zhu, Overlooked possibility of a collapsed Atlantic Meridional Overturning Circulation in warming climate. *Sci. Adv.* **3**, e1601666 (2017).